AIAA JOURNAL
Vol. 30, No. 5, May 1992

Evaluation of a Finite Volume Method for Compressible Shear Layers

H. L. Atkins*
NASA Langley Research Center, Hampton, Virginia 23665

An implicit second-order finite volume method for solving the compressible laminar Navier-Stokes equations in two dimensions is evaluated for possible use in the simulation of transitional flows. Comparisons are made with results from a spectral linear-stability code, which provides accurate growth rates, as well as perturbation eigenfunctions, for a temporally growing free shear layer. The accuracy of the growth rates of isolated modes and the physical and numerical interactions of multiple modes is the focus of this study. A grid refinement study verified the method to be second-order accurate with less than 4% error on a 32 × 64 grid. The interaction between modes of similar amplitude was small (less than 1%). In cases where there was a dominant mode, however, numerical phase error in the method pumped energy into all other modes. This numerical phase error results in nonphysical growth rates for modes whose amplitude content is several orders of magnitude below the dominant mode. When the dominant mode saturates, the pumping action ceases, and the growth rate of the next largest growing mode regains physical significance.

Introduction

In the past, the most credible stability, transition, and turbulence simulations have been performed by spectral methods[1-5] although there are many examples in which compact-support (CS) methods (including finite volume, finite difference, and finite element) were used.[6-8] Although the accuracy properties of spectral methods is unquestionable, they are difficult to apply to complex domains, and their ability to treat flows with shocks is suspect. The fundamental difference between the two is their choice of basis functions: spectral methods use a set of high-order global functions, whereas CS methods use low-order local functions (usually algebraic) coupled at cell interfaces. It seems reasonable to suppose that between the two approaches there is a middle ground that provides the needed accuracy and flexibility. In fact, this middle ground is being approached by various researchers from both directions: spectral mutidomain methods,[9] in which the global domain is subdivided and a set of basis functions are defined for each region, offer increased geometric flexibility; while from the other direction, smooth algebraic interpolation techniques (such as ENO[10]) allow many CS methods to be extended to high order (approaching global basis functions) while avoiding the oscillations that usually accompany high-order polynomials.

Although the effects of numerical diffusion and dissipation are always of concern, they are especially important in transition simulations, where the physical process being modeled is inherently unstable or the determination of the stability boundary is the objective of the simulation. While second-order-accurate CS methods are popular in most areas of fluid mechanics, transition simulations by CS methods are often fourth order. Still, their reliability is questioned, especially by those who are accustomed to the accuracy properties of spectral methods. Before embarking on a project to develop a new high-order CS method, an understanding of the capabilities and limitations of current methods is needed.

The intent of this study is to evaluate a current two-dimensional second-order finite volume Navier-Stokes code for transitional flows. This code has been used in the past to compute unsteady inviscid flows of aerodynamic interest[11,12] and has proved to be accurate and efficient in those studies. For the present study, the code was extended to treat the laminar viscous and heat conduction terms. The test problem chosen for this study is a temporally growing parallel shear layer, which is perturbed at one or more wavelengths. This choice of test problem allows comparisons with established spectral methods. This study goes into more depth than most previous validation studies of CS methods in that mode interaction and the behavior of unexcited modes is examined in addition to the usual single-mode analysis.

The first section of this paper gives a description of the governing equations and the numerical method on which the code is based. Additional information may be found in Refs. 10 and 11. The second part of this paper describes, in detail, the test problem and the diagnostic procedures used in evaluating the code's performances. In the Results section, three important cases are discussed: 1) the growth of isolated modes, 2) the interaction of modes with similar amplitudes, and 3) the interaction of modes whose amplitudes differ by several orders of magnitude.

Numerical Method

The code employs a cell-centered finite volume method for the solution of the compressible laminar Navier-Stokes equations for an ideal gas. The time integration is performed by an alternating-direction-implicit (ADI) procedure, and total-variation-diminishing (TVD) techiques are employed for spatial smoothing. The viscous terms were added to the existing Euler code, while making no modifications to the numerical smoothing inherent to the TVD operator. Formally, the method is second-order accurate for smooth grids with truncation error terms of the form (Δx^2, Δy^2, Δt^2, $\Delta x \Delta t$, $\Delta y \Delta t$).

Governing Equations

In two dimensions, the integral form of the unsteady Navier-Stokes equations can be written as

$$\frac{\partial}{\partial t}\iint_{\Omega} U \, d\Omega = -\int_{\partial\Omega}\left(F\frac{\partial y}{\partial s} - G\frac{\partial x}{\partial s}\right) ds \qquad (1)$$

Presented as Paper 89-1809 at the AIAA 20th Fluid Dynamics, Plasma Dynamics, and Lasers Conference, Buffalo, NY, June 12-14, 1989; received March 12, 1990; revision received Aug. 12, 1991; accepted for publication Aug. 19, 1991.

*Research Scientist. Member AIAA.

where Ω denotes an arbitrary region, $\partial\Omega$ is its boundary, ds is the differential element on the boundary of $\partial\Omega$, with counterclockwise being positive, and

$$U = [\rho, \rho u, \rho v, \rho e]^T$$

The density is denoted by ρ, u and v are the velocity components in the x and y directions, and e is the specific total energy. All quantities are normalized such that, for a perfect gas, the temperature is given by

$$T = (\gamma - 1)[e - (u^2 + v^2)/2]$$

where γ is the ratio of specific heats, and the equation of state is

$$P = \rho T$$

The fluxes are split into viscous and inviscid components:

$$F = F_e - F_v \qquad G = G_e - G_v$$

where

$$F_e = \begin{bmatrix} \rho u \\ \rho(u^2 + T) \\ \rho uv \\ \rho u(e + T) \end{bmatrix} \qquad G_e = \begin{bmatrix} \rho v \\ \rho uv \\ \rho(v^2 + T) \\ \rho v(e + T) \end{bmatrix}$$

$$F_v = Re_r^{-1} \begin{bmatrix} 0 \\ \tau_{xx} \\ \tau_{xy} \\ u\tau_{xx} + v\tau_{xy} - q_x \end{bmatrix}$$

$$G_v = Re_r^{-1} \begin{bmatrix} 0 \\ \tau_{xy} \\ \tau_{yy} \\ u\tau_{yx} + v\tau_{yy} - q_y \end{bmatrix}$$

$$\tau_{xx} = 2\mu(2u_x - v_y)/3 \qquad \tau_{yy} = 2\mu(2v_y - u_x)/3$$

$$\tau_{xy} = \tau_{yx} = \mu(u_y + v_x)$$

$$q_x = -Pr^{-1} \frac{\mu\gamma}{\gamma - 1} \frac{\partial T}{\partial x} \qquad q_y = -Pr^{-1} \frac{\mu\gamma}{\gamma - 1} \frac{\partial T}{\partial y}$$

The normalized viscosity is computed by a power approximation: $\mu = T^{\omega}$. The Prandtl number is denoted by Pr, and Re_r is the Reynolds number relative to the reference conditions of the variable normalization $Re_r = (\rho_r u_r l_r)/\mu_r$. In the present normalization, u_r is not a physical velocity, but instead, is defined as $u_r \equiv \sqrt{P_r/\rho_r}$. Consequently, Re_r is a numerical Reynolds number that must be computed from the physical Reynolds number and the choice of reference conditions.

Discrete Equations

Equation (1) is evaluated in each cell of the computational domain to yield a system of discrete nonlinear equations of the form

$$\Delta U_{i,j} = -\frac{\Delta t}{A_{i,j}} (\theta R(U)_{i,j}^{n+1} + (1 - \theta) R(U)_{i,j}^{n}) \qquad (2)$$

where $A_{i,j}$ is the area of cell i,j, Δt is the time step, $\Delta U_{i,j}$ is the change in U in cell i,j during the time step, and $R(U)_{i,j}^{n}$ denotes the discrete approximation of the spatial terms [the right-hand side of Eq. (1)]. The spatial terms are evaluated by defining a numerical flux for each face of the cell and then by summing around the cell:

$$R(U)_{i,j} = \Phi_{i+1/2,j} + \Phi_{i,j+1/2,j} - \Phi_{i-1/2,j} - \Phi_{i,j-1/2}$$

The numerical flux, like the physical flux, is split into viscous and inviscid components, $\Phi = \Phi_e + \Phi_v$. The numerical inviscid flux consists of a second-order average of the physical flux terms, plus a smoothing term based on the TVD methods of Harten.[13] A detailed description of the numerical inviscid flux may be found in Ref. 11.

The numerical viscous flux involves the evaluation of products of flow variables and flow gradients. The flow variables, on a face, are computed by averaging properties adjacent to the face. On a vertical face, for example: $\bar{u}_{i+1/2,j} \equiv (u_{i,j} + u_{i+1,j})/2$. The average viscosity is computed by first computing a face average temperature and then computing the viscosity from the power-law approximation. The flow gradients are computed by defining a coordinate transformation which is local to the face:

$$\begin{bmatrix} \frac{\partial}{\partial x} \\ \frac{\partial}{\partial y} \end{bmatrix} = J^{-1} \begin{bmatrix} y_\eta & -y_\xi \\ -x_\eta & x_\xi \end{bmatrix} \begin{bmatrix} \frac{\partial}{\partial \xi} \\ \frac{\partial}{\partial \eta} \end{bmatrix}$$

where

$$J = x_\xi y_\eta - x_\eta y_\xi$$

In evaluating the shear stress and heat conduction terms, face-normal gradients are computed immediately from properties on either side of the face, while face-tangent gradients must be averaged. The reverse is true for the derivatives of the coordinate transformation: coordinate derivatives tangent to the face are known immediately (and exactly), and coordinate derivatives normal to the face must be averaged. As an example, the gradients on a vertical face are

$$J(u_x)_{i+1/2,j} = y_\eta u_\xi - \bar{y}_\xi \bar{u}_\eta \qquad J(u_y)_{i+1/2,j} = \bar{x}_\xi \bar{u}_\eta - x_\eta u_\xi$$

where

$$u_\xi = u_{i+1,j} - u_{i,j}$$

$$\bar{u}_\eta = (u_{i,j+1} + u_{i+1,j+1} - u_{i,j-1} - u_{i+1,j-1})/4$$

and

$$\bar{x}_\xi = [(x_\xi)_{i,j+1/2} + (x_\xi)_{i+1,j+1/2} + (x_\xi)_{i,j-1/2} + (x_\xi)_{i+1,j-1/2}]/4$$

A similar expression is used for $\bar{y}_\xi$.

To integrate Eq. (2) in time, the spatial terms at $n + 1$ are linearized to yield a system of linear equations for ΔU.

$$R(U)_{i,j}^{n+1} \approx R(U)_{i,j}^{n} + \frac{\partial}{\partial U} R(U)\Delta U$$

$$\left(I + \theta \frac{\Delta t}{A_{i,j}} \frac{\partial}{\partial U} R(U)\right) \Delta U = -\frac{\Delta t}{A_{i,j}} R(U)_{i,j}^{n} \qquad (3)$$

The Jacobian of $R(U)$ is split by direction and simplified such that each direction attains a tridiagonal structure. Thus

$$\frac{\partial}{\partial U} R(U) \approx \zeta_\xi + \zeta_\eta$$

The simplifications involve neglecting the time change of the face-tangent components of the shear stress (cross derivatives) and the time change of the higher order components of the smoothing terms. The ADI[14] method of solution is applied by factoring the left-hand side and solving in two steps:

$$\left(I + \theta \frac{\Delta t}{A_{i,j}} \zeta_\xi\right) W = -\frac{\Delta t}{A_{i,j}} R(U)^n_{i,j}$$

$$\left(I + \theta \frac{\Delta t}{A_{i,j}} \zeta_\eta\right) \Delta U = W$$

Although the implicit method is unconditionally stable, the time step is limited for accuracy considerations. The time step is computed such that the inviscid Courant-Friedrichs-Lewy (CFL) number in each cell is less than a specified value (usually 1.0). Due to the extreme y clustering, the inviscid time step is several times larger than what would be required for an explicit method.

Test Problem and Numerical Test Procedure

For the purposes of code validation, a temporally growing shear layer was chosen as a test case. The parallel mean flow was specified as a hyperbolic-tangent profile, and the solution was forced to be periodic on a specified wavelength λ. The mean flow, shown in Fig. 1, can be described in terms of three parameters: the freestream Mach number (M_∞), the minimum streamwise wave number ($\alpha = 2\pi\delta/\lambda$), and the Reynolds number based on δ (Re_δ). For all cases presented, the Mach number is 0.5 and the Reynolds number is 200. At this Reynolds number, the instability is inviscid inflectional; consequently, this case should provide a difficult test for the numerical dissipation of the method.

The following notation is used to distinguish between the minimum wave number of the domain and its harmonics: $\alpha_1 = \alpha$, $\alpha_2 = 2\alpha$, $\alpha_3 = 3\alpha$ . . . , etc. Initial profiles of the normalized variables have the form

$$u(x,y) = \sqrt{\gamma}\, M_\infty \left\{\tanh(y/\delta) + \sum_k \beta_k Re(\hat{u}(y) e^{i(\alpha_k x + \phi_k)})\right\}$$

$$v(x,y) = \sqrt{\gamma}\, M_\infty \sum_k \beta_k Re(\hat{v}(y) e^{i(\alpha_k x + \phi_k)})$$

$$T(x,y) = 1 + \sum_k \beta_k Re(\hat{T}(y) e^{i(\alpha_k x + \phi_k)})$$

$$P(x,y) = 1 + \sum_k \beta_k Re(\hat{P}(y) e^{i(\alpha_k x + \phi_k)})$$

where $Re(x)$ denotes the real part of x, and ϕ_k and β_k are the initial phase and amplitude of the mode α_k (β_k is nonzero only for excited modes). The eigenfunctions $\hat{u}$, $\hat{v}$, $\hat{T}$, and $\hat{P}$ are obtained from a spectral linear stability program[1] which also provides the "exact" linear growth rates.

The computational domain is mapped by a rectangular grid that is uniform in x and stretched in y by the following function:

$$y(\eta) = \Gamma\eta \left(\frac{\varepsilon - 1}{\varepsilon - |\eta|}\right) \qquad -1 < \eta < 1$$

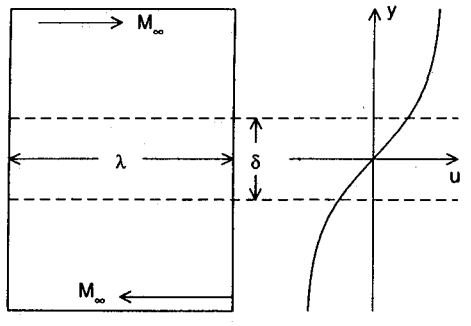

Fig. 1 Computational region and mean flow for shear flow simulation.

For most cases, the stretch parameters (Γ and ε) were chosen so that the outer boundary was at 50δ, and half of the points were within 2δ.

The natural unsteady flow resulting from the initial state described above is a shear layer that grows in thickness. The thickening of the shear layer corresponds to an α that increases in time, and thus, the growth rate of the initial mode would not be constant in time. A steady mean flow is recovered (artificially) by computing and storing the spatial derivatives of the mean flow (the mean residual). The mean residual is subtracted from the instantaneous residual at each time step of the numerical integration.

In the code used in this study, characteristic-based conditions are usually enforced at in/out flow boundaries; however, for the present study, all quantities in the far field ($|y/\delta| > 50$) were held fixed at the mean flow values. Periodicity was enforced by the use of ghost cells that extend the domain in the x direction. This allowed the discrete operator in cells next to the periodic boundary to be evaluated as if they were interior cells. The ADI algorithm did not use a periodic tridiagonal solver in the x direction. This did not cause any noticeable problems, probably because the clustering in the y direction caused the time step to be small compared to the cell size in the x direction.

The computed results are evaluated by determining the amplitude of each mode and studying its history. The amplitude of a mode (E_k) is measured by Fourier analysis of the velocity components with respect to x and then integrating in y (or summing in η).

$$\zeta_{k,j} = \frac{1}{N}\sum_{i=1}^{N} u(x_i,y_j) e^{i(\alpha_k x_i)}$$

$$\xi_{k,j} = \frac{1}{N}\sum_{i=1}^{N} v(x_i,y_j) e^{i(\alpha_k x_i)}$$

$$E_k = \frac{1}{M}\sum_{j=1}^{M} (\zeta_{k,j}\overline{\zeta_{k,j}} + \xi_{k,j}\overline{\xi_{k,j}})$$

where N and M are the number of cells in the x and y directions. The growth rate of the kth mode is given by

$$g_k = \frac{1}{2E_k}\frac{\partial E_k}{\partial t}$$

Results

Grid refinement studies were performed for two values of α: 0.2 and 0.397 (the most unstable mode[2]) on grids of 16×32, 32×64, and 64×128. In each case, the α_1 mode was excited with $\beta_1 = 0.001$. The growth rates, shown in Fig. 2, are linear in $(N_{max}/N)^2$, indicating second-order accuracy. The absolute error of a mode (ε_k) is measured in terms of the maximum growth rate as

$$\varepsilon_k = 100\,\frac{|g_k - g_{k,\text{exact}}|}{g_{max}}$$

For the case of $\alpha = 0.2$, the error is approximately 2%. The error is larger for the case of $\alpha = 0.397$; however, this case was computed on a slightly different grid which was less resolved near $y = 0$. Figure 3 shows the total vorticity obtained at saturation for $\alpha = 0.2$ on a 32×64 grid. All remaining results are for a 32×64 grid.

The method was found to be insensitive to the initial amplitude of the excited wave. For $\alpha = 0.4$, β_1 was varied from 0.1 to 10^{-7}. The instantaneous amplitudes and growth rates are shown in Figs. 4a and 4b. Over the linear region, all cases predict the same growth rates and saturate at the same amplitude, which is consistent with spectral computations performed for incompressible shear layers.[3]

The influence of α was investigated from two points of view. When the length of the domain is matched to the excited mode, as it has been in all the above cases, the error is between

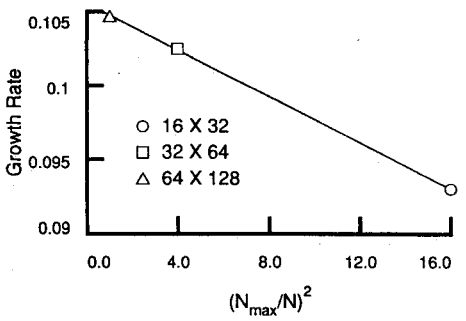

Fig. 2 Convergence of growth rate with respect to the mesh size. The method displays second-order accuracy for $\alpha = 0.2$, $\beta_1 = 0.001$.

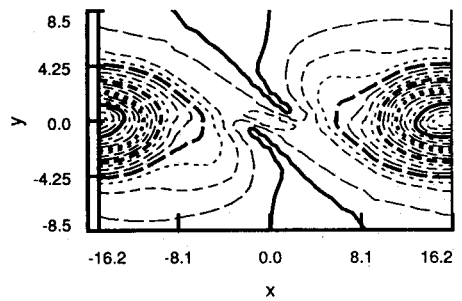

Fig. 3 Contours of vorticity at saturation for $\alpha = 0.2$: minimum contour value = 0.0, contour increment = 0.022.

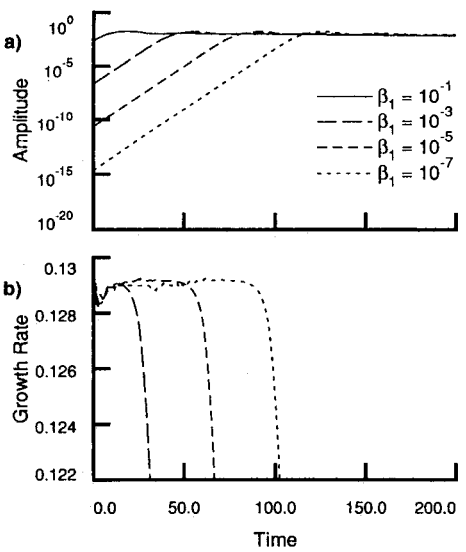

Fig. 4 Amplitudes and growth rates of the first mode for various values of initial amplitude: $\alpha = 0.4$. All cases grow at approximately the same rate and saturate at the same amplitude.

1 and 4%, similar to what was found in the grid refinement study. Figure 5 gives the growth rates and percent error for $\beta_1 = 10^{-5}$, $\alpha = 0.2$, 0.4, 0.6, and 0.8. However, when the grid is fixed at $\alpha = 0.2$ and the flow is excited at higher wave numbers, the accuracy deteriorates with increasing α_k. This is not unexpected since it corresponds to coarsening the grid in the x direction. The α_2 mode has 16 cells per wavelength and α_4 mode has eight cells per wavelength. Figure 6 shows the growth rates and percent error of the kth mode vs $(\alpha_k)^2$. The error increases linearly in $(\alpha_k)^2$, which further verifies the second-order accuracy of the method.

All the calculations described above were excited at a single mode, and evaluation of the method considered only the mode

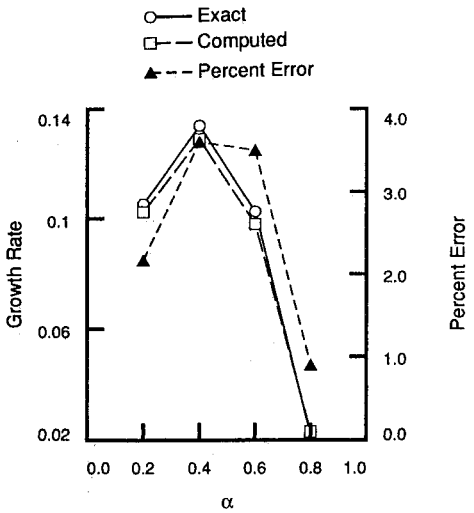

Fig. 5 Growth rate and percent error of the first mode vs the length of the domain. Error of the first mode is insensitive to α.

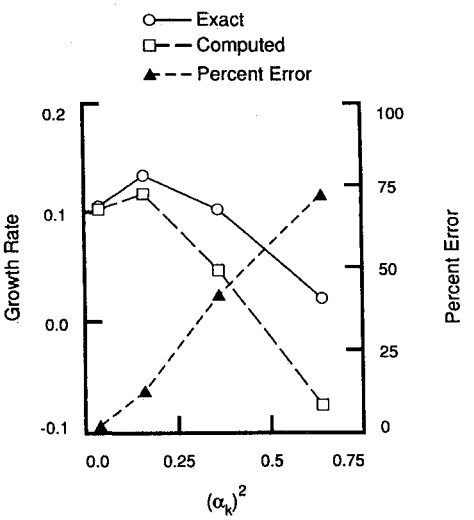

Fig. 6 Growth rate and percent error of the kth mode with domain of fixed length. Error increases as the resolution of the wave decreases.

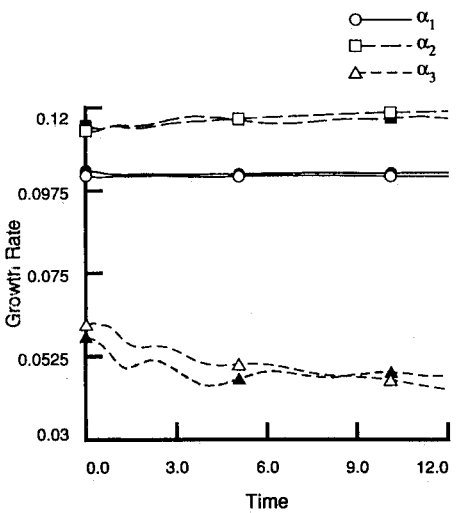

Fig. 7 Growth rates of three modes excited simultaneously (*open symbols*) compared to each mode excited separately (*solid symbols*): $\alpha = 0.2$.

that was expected to dominate. The remaining discussion examines the behavior of the unexcited modes as well as the excited modes. Also, the interaction of modes is studied by considering cases in which several modes are simultaneously excited.

In the linear region, there is very little interaction between modes excited at similar, but low, amplitudes. Figure 7 shows the instantaneous growth rates for $\alpha = 0.2$, $\beta_k = 10^{-5}$ for $k = 1, 2$, and 3, compared with the same three modes excited separately. All excited modes are growing at approximately the correct rate. Figures 8a–8d show the instantaneous amplitudes of all three modes for the four cases. Initially, the amplitudes of the unexcited modes grow very rapidly (nonphysical growth rates), but they remain several orders of magnitude below the excited mode. There is a weak coupling between the α_1 mode and the α_3 mode, and very little coupling between the α_2 mode and the other two.

In most cases, this numerical interaction does not interfere with the excited modes; however, this is not always true. In the following case, two modes are excited at different amplitudes and with varying phase relations. The grid is scaled for an α of 0.2, and the flow is excited with $\beta_1 = 10^{-5}$ and $\beta_2 = 10^{-3}$. Also, a case was computed in which the first mode ($\alpha_1 = 0.2$) was not excited. The amplitudes for the α_1 and α_2 modes are shown in Figs. 9a–9c. In the first case, Fig. 9a, the α_1 mode is in phase with the α_2 mode. The α_2 mode grows at the correct rate and quickly saturates. While the α_2 mode is growing, the growth rate of the α_1 is larger than the linear rate, indicating that some energy is being pumped into it. The growth α_1 mode stalls at approximately the same time that the α_2 mode reaches saturation, after which it interacts nonlinearly with the second mode, growing slowly to dominate eventually. Similar behavior has been observed in spectral simulations of incompressible flows.[3] In the second case, Fig. 9b, the α_1 mode is 90 deg out of phase with the α_2 mode. The initial behavior is similar to the previous case; however, after the α_2 mode saturates, the α_1 mode grows at approximately the linear growth rate until saturation. It is not clear whether the pumping action ceases when the larger amplitude mode saturates, or whether the pumping action has simply become small compared to the physical growth rate. In the third case, Fig. 9c, there is no initial excitation of the α_1 mode. After an initial stage, in which the growth rate of the α_1 mode is very large, the behavior of this case is very similar to the first case. In fact, the amplitudes of the α_2 mode for the first and third cases overlay. In all three cases, the growth rate of the α_1 mode approaches the linear growth rate just prior to reaching its final saturation amplitude, and the amplitude of the α_2 mode decreases to a new saturation state. It is at this time that the roll-up process is most evident (Fig. 10).

There are several mechanisms by which energy can be transferred into the initially unexcited modes. The equations are nonlinear, so there is a physical path for energy transfer; however, it is expected to be small in the linear region. Nonphysical mechanisms include the computer rounding error and the phase error of the numerical method. Initially, there was some concern that the Fourier analysis used in postprocessing might be interpreting the data incorrectly, and thereby producing apparent aliasing errors. The computed values are (strictly speaking) cell averages; whereas, the Fourier analysis

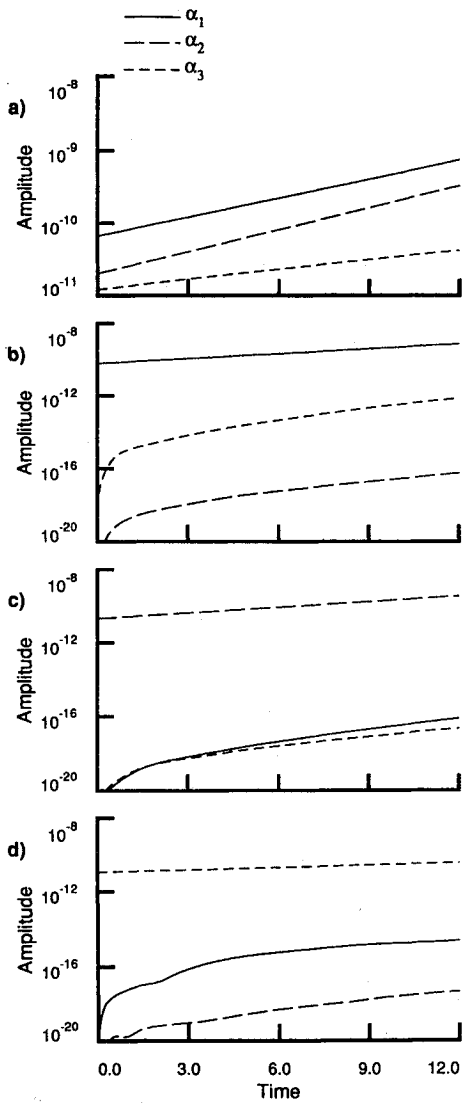

Fig. 8 Amplitudes of three modes excited simultaneously a) and the three modes excited separately: b) α_1, c) α_2, d) α_3. The α_1 mode shows a mild coupling to the α_3 mode.

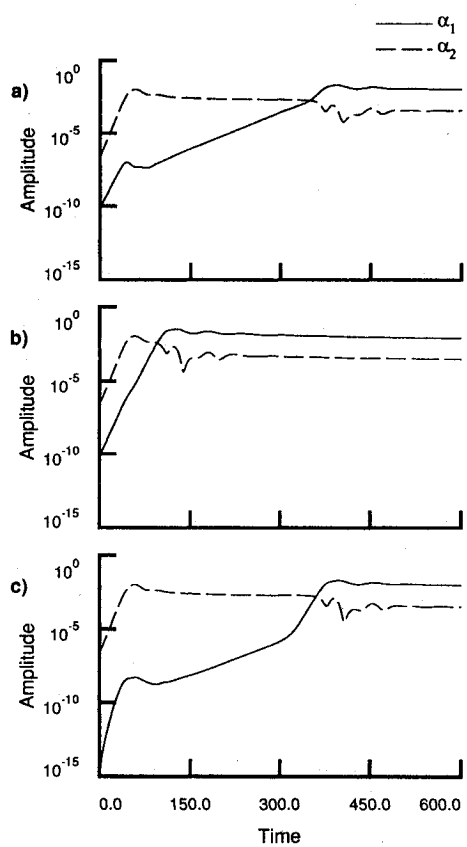

Fig. 9 Amplitudes for two modes a) excited in phase, b) excited with a phase shift of $\pi/2$, and c) no initial excitation of the α_1 mode.

treats the computed values as point values. Analysis has shown that the difference in interpretations will cause the amplitude to be different by a factor (which depends on the number of points), but that the growth rates would not be affected and aliasing errors could not arise from this procedure.

Empirical models suggest that the rapid initial growth of unexcited modes is caused by machine rounding errors that accumulate linearly in time. At later times, the growth of unexcited modes tends to parallel the largest-amplitude growing mode, indicating that numerical phase error is "pumping" energy from the large-amplitude modes to the low-amplitude modes. The rounding errors are more or less random; however, the numerical phase errors are of a periodic nature because the solution is periodic. Thus, the energy transfer due to the numerical error is coherent and much more detrimental than rounding errors. A mode will grow in a physically realistic manner whenever the amplitude of the mode ceases to be "small" when compared to all larger-amplitude growing modes.

Conclusions

A finite volume method has been verified to be second-order accurate for a temporally growing compressible shear layer. The method can accurately predict the behavior of a single perturbation of any amplitude, provided the spatial resolution is adequate; however, the numerical dissipation of the high-frequency modes (less than eight cells per wavelength) was very noticeable. The interaction of multiple modes is also well predicted, but only if the modes are excited at similar amplitudes. The method does not accurately predict the behavior of modes with amplitudes that are several orders of magnitude below that of the dominant growing mode. Computer rounding and phase error of the method "pumps" energy from the dominant mode into all other modes. If the excited mode is not the longest wave supported by the domain, the phase error will "pump" energy into the longest wavelength, causing it to dominate the flow eventually. Knowing the potential for low-order CS schemes to produce physically incorrect results, even on these simple test problems, numerical effects must be carefully identified and, if possible, ruled out through grid refinement studies when applying such methods to the simulation of complex nonlinear mode interactions. The results indicate that transition simulation may be within the capability of a high-order CS method; however, close attention should be paid to phase error as well as amplitude error during the development and validation of the method.

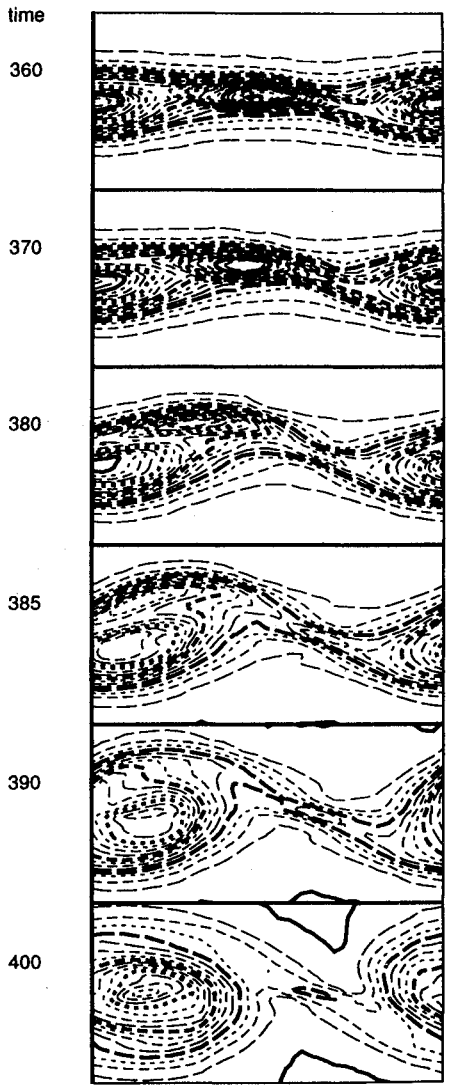

Fig. 10 Vortex roll-up for the in-phase case.

Acknowledgments

The author would like to thank C. Streett, M. Macaraeg, and M. Y. Hussaini for their time and suggestions during the course of this work.

References

[1]Macaraeg, M. G., Streett, C. L., and Hussaini, M. Y., "A Spectral Collocation Solution to the Compressible Stability Eigenvalue Problem," NASA TP-2858, Dec. 1988.

[2]Blumen, W., "Shear Layer Instability of an Inviscid Compressible Fluid," *Journal of Fluid Mechanics*, Vol. 40, Pt. 4, 1970, pp. 796–781.

[3]Metcalfe, R. W., Orszag, S. A., Brachet, M. E., Menon, S., and Riley, J. J., "Secondary Instability of a Temporally Growing Mixing Layer," *Journal of Fluid Mechanics*, Vol. 184, 1987, pp. 207–243.

[4]Zang, T. A., Krist, S. E., Erlebacher, G., and Hussaini, M. Y., "Nonlinear Structures in the Later Stages of Transition," AIAA Paper 87-1204, Honolulu, HI, 1987.

[5]Zang, T. A., and Hussaini, M. Y., "Recent Applications of Spectral Methods in Fluid Dynamics," *Large-Scale Computations in Fluid Dynamics*, Lectures in Applied Mathematics, Vol. 22, 1985, pp. 379–409.

[6]Soetrisno, M., Eberhardt, S., Riley, J., and McMurty, P., "A Study of Inviscid, Supersonic Mixing Layers Using a Second-Order TVD Scheme," AIAA Paper 88-3676.

[7]Rai, M. M., and Moin, P., "Direct Simulations of Turbulent Flow Using Finite-Difference Schemes," AIAA Paper 89-0369, Reno, NV, 1988.

[8]Lele, S. K., "Direct Numerical Simulation of Compressible Free Shear Flows," AIAA Paper 89-0374, Reno, NV, 1988.

[9]Macaraeg, M. G., and Hussaini, M. Y., *Applied Numerical Mathematics*, Special Issue on Spectral Multi-Domain Methods, Vol. 6, No. 1–2, 1989.

[10]Harten, A., Engquist, B., Osher, S., and Chakravarthy, S. R., "Uniformly High Order Accurate Essentially Nonoscillatory Schemes, III," *Journal of Computational Physics*, Vol. 71, 1987, pp. 231–303.

[11]Atkins, H., "Comparisons and Applications of Time-Accurate Finite-Volume Methods for Solving the Unsteady Euler Equations," AIAA Paper 87-1089, Reno, NV, 1987.

[12]Atkins, H., "Numerical and Analytical Study of the Inlet Startup Process in a Shock Tunnel Environment," AIAA Paper 88-0601, Reno, NV, 1988.

[13]Harten, A., "On a Class of High Resolution Total-Variation-Stable Finite Difference Schemes for Steady-State Calculations," Courant Mathematics and Computing Lab., New York Univ., DOE/ER/03077-176.

[14]Steger, J., "Implicit Finite-Difference Simulation of Flow About Arbitrary Two-Dimensional Geometrics," *AIAA Journal*, Vol. 16, No. 7, 1978, pp. 679–686.